Proton-Boron Fusion In Femtosecond-Laser-Irradiated Nanowire Array Target*

Putong Wang,[1,2,†] Jiancai Xu,[3,†] Guoqiang Zhang,[4,1,‡] Xiangai Deng,[5] Youjing Wang,[5] Zhiguo Ma,[5] Changbo Fu,[5] Lulin Fan,[3] Qingsong Wang,[3] Tongjun Xu,[3,§] Liangliang Ji,[3] Rongjie Xu,[3] Jinfeng Li,[3] Xiaoming Lu,[3] Baifei Shen,[3,6] Yancheng Liu,[1] Weifu Yin,[1,2] Xuesong Geng,[3] Hui Zhang,[3] Yuxin Leng,[3] Ruxin Li,[3] and Yu-Gang Ma[5,1,¶]

[1]*Shanghai Institute of Applied Physics (SINAP), Chinese Academy of Sciences (CAS), Shanghai 201800, China*
[2]*University of Chinese Academy of Sciences (UCAS), Beijing 100049, China*
[3]*State Key Laboratory of High Field Laser Physics and CAS Center for Excellence in Ultra-intense Laser Science, Shanghai Institute of Optics and Fine Mechanics (SIOM), Chinese Academy of Sciences (CAS), Shanghai 201800, China*
[4]*Shanghai Advanced Research Institute (SARI), Chinese Academy of Sciences (CAS), Shanghai 201210, China*
[5]*Key Laboratory of Nuclear Physics and Ion-Beam Application (MOE), Institute of Modern Physics, Fudan University, Shanghai 200433, China*
[6]*Department of Physics, Shanghai Normal University, Shanghai 200234, China.*

In this work, we performed an experimental campaign to study α-particles from laser-driven proton-boron fusion on nanowire array targets. An ultra-intense laser was utilized with an intensity of 2×10^{20} W/cm^2 to interact with nanowire array targets fabricated from a mixture of polyethylene (CH_2)n and boron carbide (CB_4) nano-powders. To reduce the proton sensitivity of CR-39 and enhance the accuracy of α-particle measurements, a Potassium-Ethanol-Water (PEW) solution was employed to treat the CR-39 detector. Furthermore, a Particle-In-Cell (PIC) code with improved nuclear reaction cross-sections was applied to calculate the proportion of α-particles directly generated by the Z-pinch effects. Our findings indicate that the direct contribution of Z-pinch from individual nanowires to the total nuclear reaction yield is relatively low. Instead, the pinch effects acclerate the original energetic ions from a shock, which contribute most of the fusion yield through collisions with the ions from other wires. A yield of 3.3×10^{6} α/J from p-B fusion was recorded, consistent with the theoretical prediction.

Keywords: p-B fusion, nanowire array target, laser induced nuclear reaction, Z-pinch

I. INTRODUCTION

The nuclear reaction between hydrogen (proton) and boron, $p+^{11}B\rightarrow 3\alpha+8.6$ MeV (p-B), has received extensive experimental and theoretical research in the past[1–4]. This reaction is not only of research interest in astrophysics[5] but also holds potential value in fusion energy applications. p-B fusion, offering clean energy without harmful neutron radiation, has gained significant attention in recent years[6–9]. Moreover, The abundance of boron on Earth is much greater than tritium, making fuel acquisition significantly easier. Since only charged particles are generated in p-B fusion, it has the advantage of sustaining energy within the plasma system. With development of ultra-intense lasers, laser fusion based on p-B driven by lasers has become a possibility. However, the reaction rate of p-B fusion is much lower than that of deuterium-tritium fusion commonly used in inertial confinement fusion (ICF). Under high-temperature thermal equilibrium conditions, the bremsstrahlung radiation loss also prevents p-B fusion from sustaining its energy output[10]. These issues can be further overcome by using ultra-short, intense lasers to drive p-B fusion out of thermal equilibrium conditions, with a much shorter timescale than ICF[11, 12].

In recent years, the efficiency of alpha production in p-B experiments driven by ultra-intense lasers has gradually improved. In experiments conducted on boron-rich polyethylene planar targets irradiated by a laser on the Moscow Neodymium facility, a yield of 10^4 α/J was reported[13]. With the PICO2000 laser facility at LULI laboratory, a 20 J laser was employed to accelerate protons to irradiate a boron-plasma target preheated with a 400 J nanosecond laser, achieving a yield of approximately 10^5 α/J alpha particles[14]. The experiment performed at the PALS achieved a yield of 10^6 α/J with a spatially well-defined layer of boron dopants in a hydrogen-enriched silicon target (Si-H-B)[15], and a yield of 10^8 α/J with a thick Chemically hydrogenated BN target[16]. Besides experiments performed on LFEX observed yields of 10^6-10^7 α/J[17, 18]. Researchers at Peking University adopted an inverse dynamics approach. The femtosecond joule laser, CLAPA, was used to accelerate boron-particles and bombard them on a plastic target. A yield of 10^6 α/J[19] was achieved. The yield up to 10^8 α/J has been measured via the pitcher-catcher scheme in plasma, which was carried out in XG-III laser facility[20].

The nanowire array (NWA) target is a near-solid-density target with a periodic structure. Its strong laser energy absorption capability has been demonstrated in both theoretical and experimental studies[21–24]. Under ultra-intense laser irradiation, Z-pinch effect induced by return currents further increases the density and energy of the particles[25].The interaction between the magnetic field and the current creates a radial Lorentz force, which compresses the plasma radially

* Supported by the Strategic Priority Research Program of the CAS (No. XDB16), the National Key R&D Program of China (2022YFA1602200, 2022YFA1602400), and the National Natural Science Foundation of China (No. 12235003).

† These authors contributed equally to this work.
‡ zhangguoqiang@sari.ac.cn
§ tjxu@siom.ac.cn
¶ mayugang@fudan.edu.cn

to a small volume[26]. This makes it possible to achieve p-B reactions which has a higher temperature thresholds than deuterium-deuterium fusion within the nanowires. In addition, the high-density plasma environment generated by the NWA may facilitate alpha re-heating, enhancing the fusion reaction rate[27, 28]. Curtis et al. conducted the deuterium-deuterium fusion experiment in NWA targets. They used femtosecond laser irradiation on deuterated polyethylene nanowire array targets, achieving higher plasma temperatures and densities. Ultimately, a neutron yield of up to 10^6 neutron/J was obtained [29, 30]. We are confident that the laser-induced p-B reactions in NWA targets will exhibit high efficiency. This belief is grounded in the NWA's ability to create the necessary conditions for p-B fusion, including the high plasma densities and temperatures required for such reactions to occur effectively.

In this work, we detail the p-B fusion process and the generation of α-particles generated using a nanowire array target on a femtosecond petawatt laser system. The α-particles generated from $p + ^{11}B \rightarrow 3\alpha$ were detected and quantified with CR-39 solid track detectors. To delve into the dynamics of alpha particle generation, we used Particle-In-Cell (PIC) simulations to assess the contribution of the Z-pinch effect to the direct production of alpha particles. Our findings indicate that while the Z-pinch effect's role in generating alpha particles from individual nanowires is comparatively minor, it significantly enhances the energy of ions originating from an initial shock. These accelerated ions then interact with ions from other wires, leading to a substantial contribution to the overall fusion yield through subsequent collisions in the later stages of the process. This insight highlights the pivotal role of pinch effects in amplifying the efficiency of the fusion reactions within the nanowire array target.

II. EXPERIMENTAL SETUP

A. Laser Parameters

The experiment was carried out on a femtosecond petawatt laser system at Shanghai Institute of Optics and Fine Mechanics(SIOM). The schematic diagram of the experimental layout is shown in Fig.1. This Ti-Sapphire laser is based on the standard chirped-pulse-amplification(CPA) technique, which deliverd laser beams with a central wavelength of 800 nm and a duration of 40 fs. As shown in Fig.2, The 5 J laser energy was focused on a 10 μm full width at half maximum(FWHM) focal spot with an F/4 off-axis parabola, which is reaching a peak laser intensity about 2×10^{20} W/cm^2 with a contrast of amplified spontaneous emission pedestal ranging from 10^{-10} to 10^{-9} at 10 ps before the main pulse[33]. The corresponding normalized laser amplitude $a_0 = 10$ ($a_0 = eE/m_e c\omega$), was calculated using e the electron charge, m_e electron mass, E the laser electric field, ω the laser frequency and c the speed of light in vacuum.

B. Diagnostic Tools

The α-particles generated from proton-Boron reaction were detected by Columbia Resin No. 39 (CR-39). This detector, known for its sensitivity to ions and immunity to background noise such as electrons and photons, has become a staple in the identification of charged particles within laser-plasma settings[34, 35]. To refine the specificity of CR-39 for our study on the laser-induced $^{11}B(p,\alpha)2\alpha$ reaction, we use a Potassium-Ethanol-Water (PEW) etching solution. This treatment effectively elevated the detection threshold, thereby reducing the detector's sensitivity to protons. For detailed methodologies pertaining to the use of the CR-39 detector, we direct the reader to our earlier publication[36, 37].

The CR-39 detectors were placed at the normal direction of in front of the target, with a spearation distance of 46 cm. To prevent interference from low-energy ions, the CR-39 sheets were encased in 10-μm-thick aluminum foils. Simulations utilizing the Stopping and Range of Ions in Matter (SRIM) software[38] indicated that the minimum energy required for an alpha particle to penetrate a 10-μm-thick aluminum foil is 2.9 MeV. Consequently, alpha particles leaving from the proton-boron interaction were capable of penetrating the foil and leaving a discernible trace in the CR-39 detector post-etching. Furthermore, the minimum energies required for protons, boron, and carbon to achieve such penetration are 0.8 MeV, 9.5 MeV and 12 MeV, respectively. The linear energy transfer calculated from SRIM allow us to distinguish between these particles using the PEW-25 etching solution[36].

The energy spectra of the ions were measured by two Thomson parabola spectrometers (TP). These spectrometers were positioned at distances of 49.6 cm and 22 cm from the target, with incident angles of 15° and 58° relative to the target normal, respectively. To prevent signal saturation, with an aperture of 100 μm diameter was integrated in front of each spectrometer, which defined the solid angles for ion collection as 3.2×10^{-8} steradians (Sr) and 1.6×10^{-7} Sr. The ion data were captured on image plates (IP). Complementary to these, additional detectors, as depicted in Fig. 1 were configured for the detection the time of fly (TOF) of neutrons. CPTOF is the gated fiber detector for laser-induced strong electromagnetic pulse environments[39].

C. Proton-Boron Targets

The nanowire array (NWA) target, designed for the $p + ^{11}B \rightarrow 3\alpha$ reaction, was fabricated with a composite material consisting of polyethylene $(CH_2)_n$ and boron carbide (CB_4) powders, in a mass ratio of 1.86:1. The atomic ratio of ^{11}B to ^{10}B was maintained at 4:1. The NWA target fabrication process commenced with heating polyethylene sheets to a molten state, followed by thorough mixing with boron carbide nanopowder. After cooling, the mixture was compacted into a dense sheet. This polyethylene-boron composite sheet was then adhered to an anodized aluminum oxide (AAO) template, which featured hexagonally arranged nano-channels. The dimensions of the NWA—diameters, lengths, and inter-

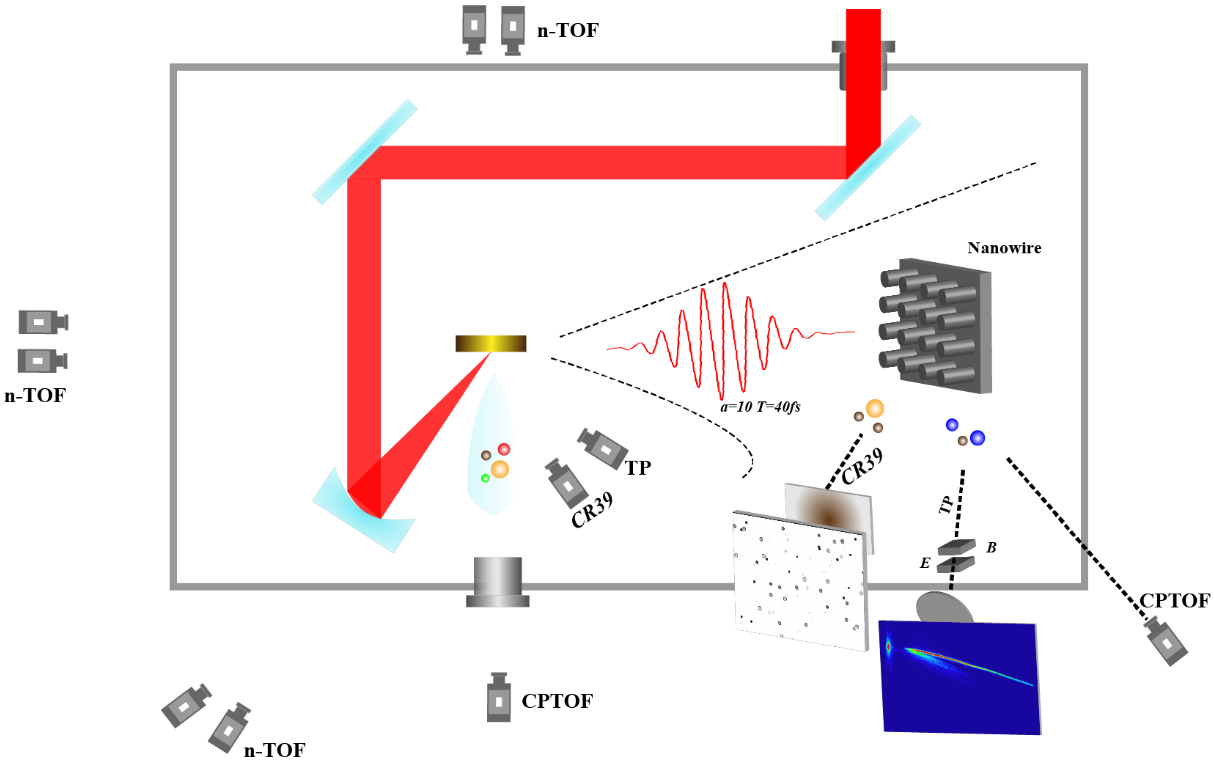

Fig. 1. Experimental setup. The laser pulses irradiate on nanowire array target with an angle of 26°

.

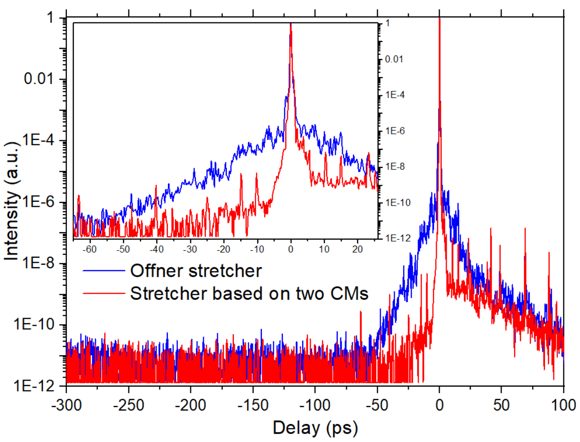

Fig. 2. The temporal distribution of the laser pulse.[31–33]

wire spacing—were dictated by the AAO template specifications. Subsequent heating and mechanical compression facilitated the infiltration of the polyethylene-boron mixture into the template's channels. Given that the average diameter of the boron carbide powder was less than 10 nm, it was significantly smaller than the nano-channel diameter. The NWA target was ultimately obtained by dissolving the AAO membrane in a sodium hydroxide (NaOH) solution for 2 hours. The substrate supporting the NWA had a thickness of approximately 300 μm. Additionally, NWA targets fabricated from deuterated polyethylene $(CD_2)_n$ sheets were prepared for the $D+D \rightarrow n+^3He$ reaction experiments. The solid density of the NWA was found to be between 17% and 36% of that of a planar target. The morphology of the NWA was examined using scanning electron microscopy (SEM). As depicted in Fig. 3(a), the center-to-center distance (S) between the wires was 800 nm, with wire diameters (D) of 500 nm and lengths (L) of 3 μm. Furthermore, NWA targets with parameters of S = 450 nm and D = 200 nm were also produced.

III. EXPERIMENTAL RESULTS

The absolute energy spectra of protons can be derived from our Thomson parabola spectrometers (TP), as referenced in our previous work[40]. We measured protons with a maximum energy of 16 MeV, which were accelerated by a target normal sheath acceleration (TNSA) field at the target front. It was confirmed that the use of a nanowire array (NWA) target significantly enhanced the ion energy compared to that of a flat target. Although our experiment measured a maximum proton equivalent temperature of approximately 800 keV, it is believed that these are emitted protons, as discussed in reference[41]. The energy proportion of these emitted protons in the plasma is considerably lower than that of confined protons. Predominantly originating from the front surface of the NWA target, these protons have a reduced likelihood of colliding with other ions, making them less

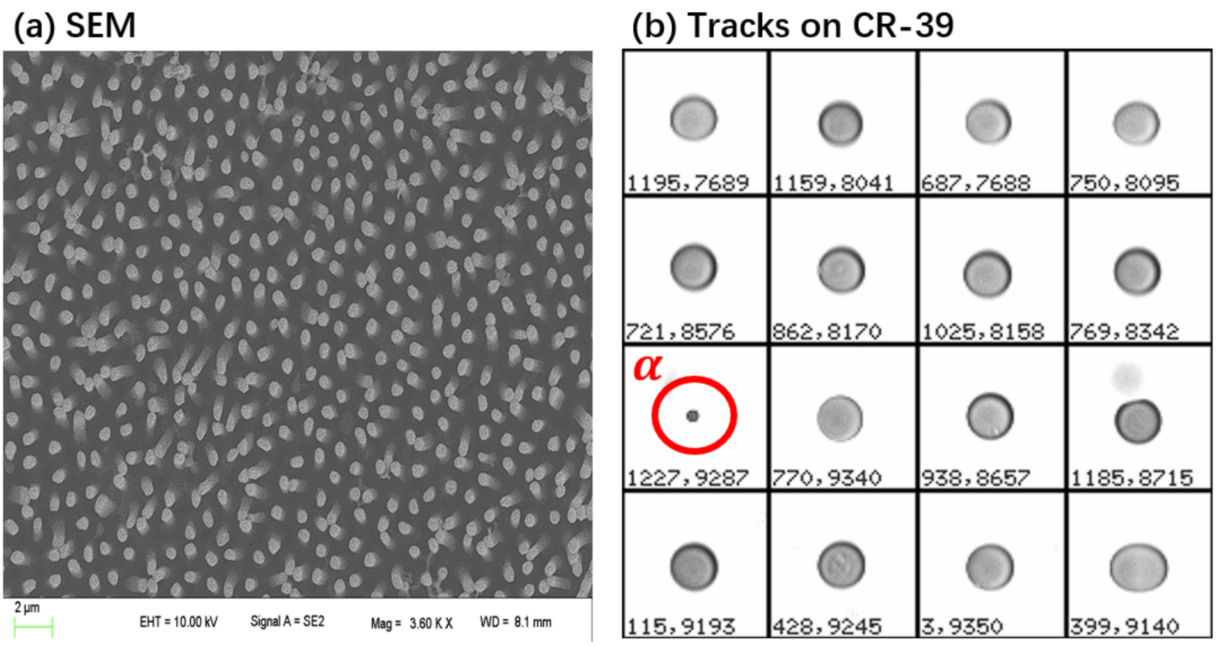

Fig. 3. (a) SEM image of nanowire array target.(b) Tracks on CR-39 after etching in the PEW-25 solution. [36]

likely to contribute significantly to nuclear reactions within the NWA. This hypothesis is further supported by the significant difference in equivalent temperature between emitted protons (300 keV) and confined particles (50 keV) noted in the reference[41]. Consequently, in the discussion section, simulation results will be utilized to analyze the energy spectrum. In our subsequent 3D particle-in-cell (PIC) simulations, confined protons exhibit an equivalent temperature of around 260 keV, as illustrated in Fig. 7. It is noteworthy that since the protons gain energy driven by the Z-pinch effect, their energy spectrum is highly non-equilibrium.

Table 1. The yield of α in our experiment

Run#	D(nm)-L(μm)-S(nm)	laser on target (J)	α yield ($\times 10^6$)
9	200-5-450	4.7	15.5 ± 5.8
15	200-3-450	3.0	6.3 ± 2.4
22	500-3-800	2.9	7.6 ± 2.6
31	500-3-800	4.0	13.1 ± 4.3
38	500-3-800	3.0	5.4 ± 2.0

CR-39 was irradiated with laser-accelerated protons, boron, carbon, and a small number of secondary α-particles of interest. The 10 μm thick aluminum foils effectively blocked low-energy particles, particularly boron and carbon, reducing their penetration into the CR-39. Protons, being easily accelerated to high energies, are challenging to distinguish from α-particles. The CR-39 sheets employed for α-particle measurements were etched in PEW-25 solution at a temperature of 60 °C for either 30 or 40 minutes, which corresponds to a suitable detection energy range for α-particles generated from the $^{11}B(p,\alpha)2\alpha$ reaction. In comparison to the NaOH-etched CR-39, the use of PEW solution significantly reduced proton tracks[36]. The track observed in Figure 3(b), highlighted in red, was generated by an α-particle, while the other tracks are attributed to heavier ions. Tracks with diameter ranging from 16-24 μm associated with heavier ions such as boron and carbon, are significantly larger than those produced by α-particles with diameters of 4-8 μm, facilitating their differentiation. Assuming that the secondary α-particles resulting from nuclear reactions are emitted isotropically, we apply a solid angle correction (the corresponding solid angle for CR-39 was 4.27×10^{-4} Sr). By counting the number of α-particles on CR-39, the results are tabulated in Table 1. Furthermore, the maximum neutron yield from the deuterated polyethylene NWA target in our experiment reached 1.3×10^7. Other neutron yields are concentrated around the order of 10^6. These measurements were conducted using the neutron time-of-flight (n-TOF) detectors illustrated in Fig. 1.

IV. SIMULATION TOOL AND SETTINGS

The Particle-in-Cell (PIC) approach has been extensively employed for simulating plasma physics phenomena since the 1970s. Over the past decades, the PIC method has undergone progressive enhancements to incorporate effects such as collisions, ionization, Quantum Electrodynamics (QED), and more. Smilei is a PIC code for plasma simulation that provides capabilities for nuclear reaction simulations [42]. Nuclear reactions may occur during collisions when specified. The reaction scheme is largely inspired by the works in ferences[43, 44].

A. Nuclear Reaction in Smilei

Although Smilei offers a comprehensive calculation for the $D+D \rightarrow n+^3He$ nuclear reaction, the final results have been found to be inaccurate due to discrepancies in the coordinate handling within its nuclear reaction module. To address this issue, we have implemented modifications to the nuclear reaction section of Smilei to ensure that the number of nuclear reaction yields aligns with theoretical predictions. To validate the precise implementation of the nuclear fusion reaction, we conducted simulations within a box system, employing both 2D and 3D configurations with periodic boundary conditions, as well as 1D collision tests. These simulations enable us to compare the outcomes against the theoretical threshold set by the reaction rate $< \sigma v >$, which characterizes the efficiency of fusion combustion.

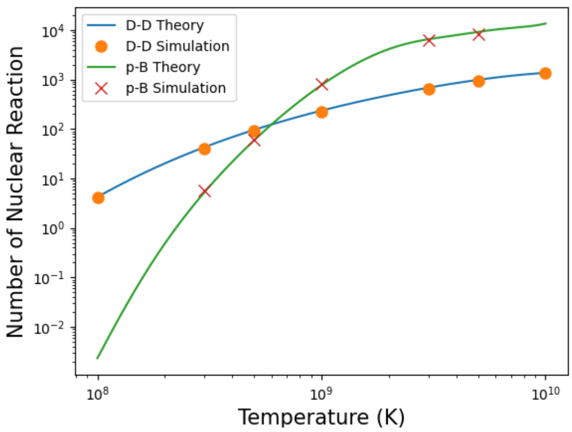

Fig. 4. Validation of the Enhanced nuclear reaction module in SMILEI. The nuclear reaction yields from D-D and p-B are calculated within a box with the sensitivity to temperature variations.

B. 3D Periodic Tests and Nuclear Reaction Validation

Our 3D periodic tests were conducted within a cubic simulation box of volume $V = 1 \times 1 \times 1 \mu m^3$. The box system was discretized into a grid of $128 \times 128 \times 128$ cells, with each cell measuring approximately 7.8 nm on each side. The deuterium density was set to $\rho = 10^{22} cm^{-3}$, which is consistent for hydrogen and boron, with a timescale of $t = 200\, fs$ and varying temperatures. Deuterium particle velocities were initialized following the Maxwell-Boltzmann distribution.

Due to the periodic boundary conditions, the velocity distribution of deuterium particles remains nearly unchanged as they evolve over time. Consequently, the fusion reaction rate $< \sigma v >$ remains relatively constant over time. This allows us to employ both theoretical analysis and computational methods to validate the accuracy of the nuclear reaction quantities. The theoretical results and simulations for nuclear reaction yields at different temperatures are presented in Figure 4. Additionally, we performed 2D periodic tests and 1D beam-target tests, with simulations consistently matching theoretical results. Reactions such as $D+D \rightarrow n+^3He$, $p+^{11}B \rightarrow 3\alpha$, and $D+^{11}B \rightarrow n+^{12}C$ were input into Smilei, and the results were verified for accuracy. In this paper, we focus on the $p+^{11}B \rightarrow 3\alpha$ reaction.

C. Simulation Settings

To elucidate the interaction of NWA targets with relativistic femtosecond pulses, we conducted 3D PIC simulations using the SMILEI code. Here, we outline the simulation parameters corresponding to our experimental setup. In this description, the x-axis denotes the axial direction of the NWA target, coinciding with the direction of laser propagation. The y-axis and z-axis are perpendicular to the laser propagation direction. As an illustrative example, we consider a NWA with a diameter (D) of 200 nm, center-to-center distance (S) of 450 nm, and length (L) of 3 μm, which is the smallest in our experimental series.

The particle number density of hydrogen is set to $\rho = 6.8 \times 10^{22}\,\mathrm{cm}^{-3}$, and the initial temperature of the particles is maintained at 300 Kelvin. Given the potential significance of the pinch effect in the nanowires [45], a fine cell size is necessary to resolve the pinched plasma at a radius of approximately 30 nm. Consequently, the cell dimensions are set to 8.5 nm $\times$ 6.75 nm $\times$ 6.5 nm throughout the simulation. The grid is configured with $576 \times 200 \times 240$ cells, and within each cell, 15 hydrogen, boron, and 5 carbon macro-particles are initialized. The nanowires are arranged in a hexagonal pattern.

The NWA target is irradiated by 800 nm wavelength laser pulses with a full width at half maximum (FWHM) duration of 40 fs. A linearly polarized laser pulse is focused to a field strength of $a_0 = 10$ at the end of the wire. The focal spot size is $10\,\mu m$, which is sufficiently large to encompass the entire simulation region. Electromagnetic boundary conditions and particle boundary conditions are set to absorbing on the x-axis and periodic on the others. Field ionization, a crucial process in the interaction between ultrahigh-intensity lasers and plasmas, is enabled within our simulation. Since field ionization overwhelmingly dominates over ionization from Coulomb collisions between particles, these Coulomb collisions are deactivated to conserve simulation time. However, nuclear collisions remain included in the simulation. Radiation effects are not considered in this simulation.

V. SIMULATION RESULTS AND DISCUSSIONS

A. Laser Induced Z-pinch

When a single wire is irradiated by ultrashort, high-intensity laser pulses, the atoms within the wire undergo field ionization. This ionization process results in a significant potential difference across the nanowire's surface, which is counterbalanced by a substantial return current flowing along

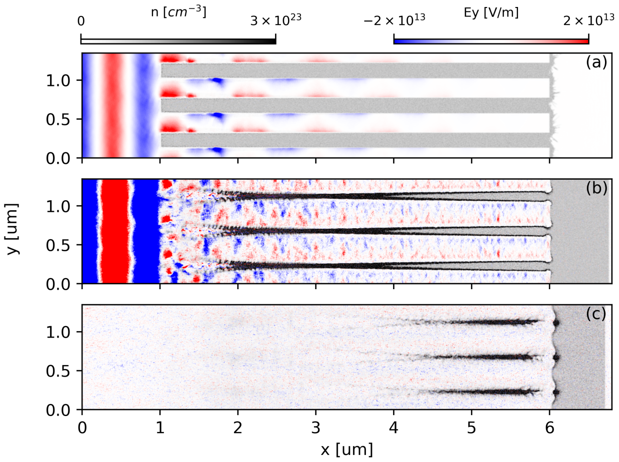

Fig. 5. Snapshots of laser-induced Z-pinch process. (a)(b)(c) are snapshots of 20 fs, 65 fs and 120 fs, respectively. The plasma density(n) spans from 0 to 3 $\times$ 10^{23} cm^{-3}. The electric field in y direction E_y fluctuates between from -2$\times 10^{13}$ to 2$\times 10^{13}$ V/m.

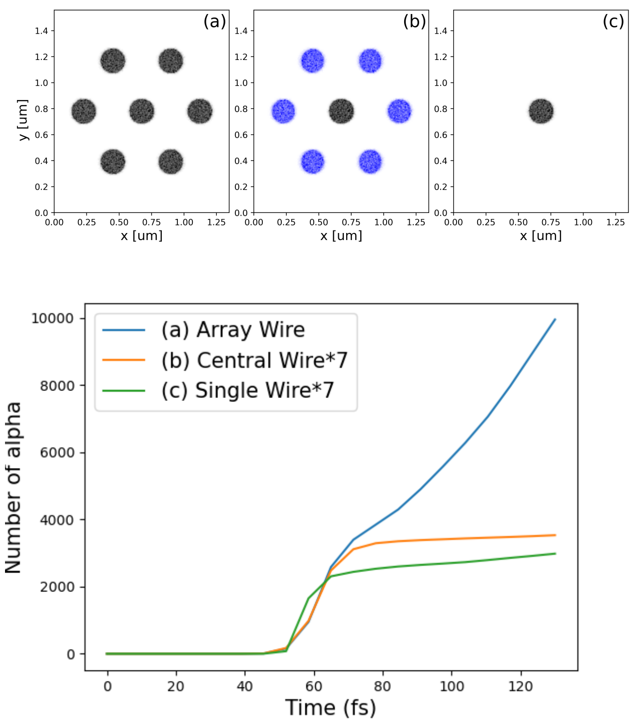

Fig. 6. The yeild of alpha from three simulation schemes. (a) Normal nanowire array (blue curve).(b) Mix nanowire array. Only real protons and borons in central wire can yield alpha (orange curve), while the other blue wires have psudo-particles, solely contribute to the density of plasma. (c) Single nanowire (green curve).

the surface to maintain quasi-neutrality. Electrons are evacuated by the laser, creating a void, while the positive current density represents the return current of electrons flowing in the opposite direction. The return current density reaches $J = 10^{15} - 10^{16} A/cm^2$. Due to this extremely high current density, the induced magnetic field around the nanowire is also substantial, with a maximum field strength of $B_y = 1.0 \times 10^6 T$. This quasi-static magnetic field exerts a $J \times B$ force on both the inner and outer currents (electrons) of the nanowire. The current on the inner surface of the nanowire is subjected to a radially inward force due to the generated magnetic field, while the forces on the outer electrons are directed oppositely. Consequently, the nanowire is compressed inward, and electrons extracted from the nanowire are pushed outward. This phenomenon is known as the Z-pinch.

The Z-pinch dynamics are depicted in Fig. 5. As the return electrons experience radial compression by the Lorentz force, they generate an electric field resulting from charge separation. Consequently, ions are attracted and symmetrically pinched inward from the surface by this induced electric field, culminating in the formation of a shock front. This shock front evolves inwardly, and within approximately 50 femtoseconds, it reaches the center of the nanowire, where the diameter is most compressed to around 30 nm. The maximum proton density at this point can surpass the initial density by a factor of over 100. It is during this critical moment that energetic ions collide with one another in the most densely populated region. Owing to the exceedingly high particle number density, nuclear reactions are predominantly concentrated around the axis of the nanowire. The extremely brief compression phase results in a burst of reactions occurring within femtoseconds.

B. Tracing the Contribution of Nuclear Fusions

To ascertain the contribution of nuclear fusions, we designed three distinct simulations to investigate the role of the Z-pinch under our experimental parameters. The first simulation features seven nanowires arranged in a hexagonal pattern, mirroring the configuration of our experimental target. The second simulation, an extension of the first, designates only the central nanowire as capable of undergoing nuclear reactions with protons and boron, while other nanowires are inert to such reactions. The third simulation isolates a single nanowire in space. The initial configurations for these scenarios are illustrated in Fig. 6(a), (b), and (c), respectively. The blue curve in Fig. 6 corresponds to the α yield in scenario (a). The orange and green curves represent seven times the α yields for scenarios (b) and (c), respectively. The transient burst of α particles between 50 fs and 80 fs is attributed to the Z-pinch effect. Comparing the outcomes of (a) and (b), we find that the number of α particles generated during the Z-pinch phase is nearly identical. However, the yield from interactions among different wires in scenario (a) shows a sharp and sustained increase afterward. This divergence is anticipated to be more significant in our larger-scale experiments, implying that the Z-pinch may have a limited impact on the overall nuclear reactions within the nanowire array target setup. The contrast between the results of (b) and (c) sug-

gests that the NWA target is more effective at inducing a Z-pinch compared to a solitary wire in vacuum conditions (or a sparse NWA target). In our simulations, we observed that the shorter the wire length, the more pronounced the difference between scenarios (b) and (c). The close spacing between nanowires allows electrons to fill the interstitial gaps, hindering the laser from penetrating deeply, as depicted in Fig. 5. This reduction in ionization and electron loss at the wire termini leads to a more substantial return of electrons, thereby amplifying the Z-pinch effect. Consequently, scenario (b) exemplifies an ideal case of a Z-pinch driven by the laser. The Z-pinch effect could account for the high laser energy absorption efficiency observed in nanowire arrays. Moreover, the shock induced by the Z-pinch is a pivotal pathway for ion energization. Despite these insights, the Z-pinch directly catalyzes only a limited number of nuclear reactions under our experimental conditions.

Therefore, we conclude that the nuclear reactions in our experiment can generally be divided into two parts. Initially, the interaction between the NWA target and the femtosecond laser produces an alpha (neutron) burst due to the Z-pinch. However, this burst constitutes only a small fraction of the total reaction yield. It is followed by a prolonged and steadily generated nuclear reactions from plasma expansion. Eventually, these ions will diffuse into the vacuum or target. The short pulse width and small scale of Z-pinch require other parameters to be emphasized, such as using sparse array targets and tight focusing. We have another work focused on the theoretical study of a single wire and Z-pinch in them.

C. Estimation of Total α-Particle Yield and Efficiency

Nuclear reactions predominantly driven by plasma expansion, which exceed the timescale resolvable by PIC simulations, suggesting that these simulations may be hard to capture the entire physical process. Within the simulation parameters outlined in this section, the NWA target yields approximately 6×10^4 α particles at 300 fs. Even if we assume unitary laser energy distribution within the focal spot (this estimation may be likely to 2-3 times higher than the gaussian distribution of a real laser spot), the projected total number of α particles generated is around 10^6, which remains lower than the counts observed in our experiments.

To estimate the total α-particle yield from the reactions, we integrate the particle energy spectrum obtained from PIC simulations, with the SRIM data and the cross-section for the $p+^{11}B \rightarrow 3\alpha$ reaction, as depicted in Fig.7. It is important to note that the energy spctrum is the original one which will be refined through the subsequent SRIM calculation. Our simulation results indicate an α-particle yield of 2.3×10^7. Consistent with our experimental results in Table.1, the number of α-particles in 4π is $\sim 1.6\times10^7$. An efficiency of $3.3\times10^6\alpha/J$ with our femtosecond petawatt laser system has been detected. Taking into account the values from our theoretical simulations for all α-particles, the yield has the potential to $4.9\times10^6\alpha/J$, given the optimization of target fabrication processes and the refinement of CR-39 measurement

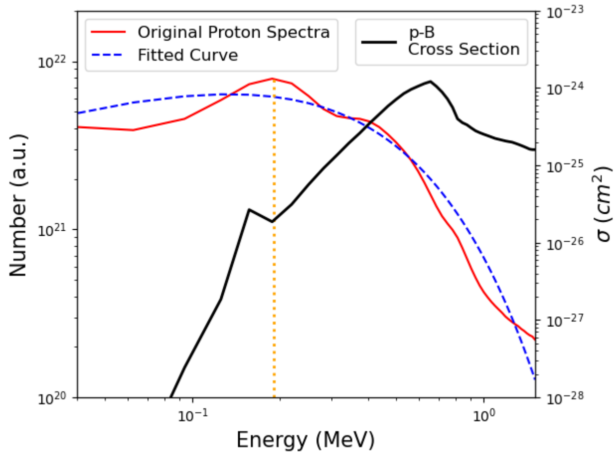

Fig. 7. Proton spectrum from 3D PIC simulation and the cross-setion of p-B from experiment. The red curve is original proton spectrum. The blue curve is fitted curve. The orange dot line is 0.19 MeV.

techniques.

Using the same methodology to estimate the neutron yield, we obtain a result of 1.0×10^7. This aligns with the highest overall yield of 1.3×10^7 observed in our experiment and consistent with the result from the pioneering works[29, 30]. Therefore, employing higher-energy lasers to induce p-B reactions in NWA targets is expected to be more efficient than D-D reactions.

Increasing the energy of the laser deposited into the NWA target enhances the energy of the confined particles, which in turn boosts the total reaction yield. As illustrated in Fig. 8, our simulation exteneded to 15 J, have demonstrated an α yield reaching up to 10^8. Furthermore, optimizing target parameters could potentially enable the Z-pinch effect to more effectively convert laser energy into ion energy. For instance, simply increasing the length of the wire in PIC simulations results in a linear increase in the number of nuclear reactions, at least within a length of 15 μm.

VI. CONCLUSION

In summary, we report an experimental measurement of a α-particle yield of $3.3\times10^6\alpha/J$ using a nanowire array target on the femtosecond petawatt laser system at SIOM for the first time. This yield is consistent with the theoretical simulations based on PIC, the stopping power from SRIM, and the nuclear reaction cross-section for proton-boron fusion. We employed the PEW solution to etch CR-39, facilitating the detection and distinction of α-particles generated by the p-B fusion.

Utilizing our enhanced SMILEI nuclear reaction simulation code, we calculated the total α yield following the interaction of the laser with the target over a few hundred femtoseconds, specifically determining the proportion of α-particles directly generated by the Z-pinch. The results indicate that, under our experimental parameters, the direct con-

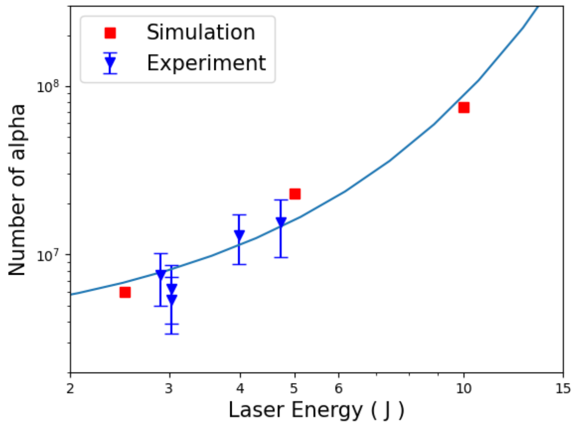

Fig. 8. Alpha yield as a function of laser pulse energy on NWA target. The curve shows a trend based on simulation and experimental results.

tribution of the Z-pinch to the total nuclear reaction yield is relatively low. However, we posit that the shock driven by the Z-pinch is a pivotal mechanism for ion energization.

Our investigation into p-B nuclear reactions in nanowire array targets contributes to the understanding of the unique fusion platform driven by nanostructured arrays irradiated with intense, ultra-short laser pulses [46]. The α-particles emanating from these fusion reactions occur within a minuscule spatial and temporal scale, potentially contributing to a robust-particle source suitable for a myriad of applications. Moreover, the high-density and intense-field plasma environment created by the nanowire may amplify the fusion cross-section [47], potentially improving the efficiency of nuclear reactions.

ACKNOWLEDGMENTS

This work was supported by the Strategic Priority Research Program of the CAS (No. XDB16), the National Key R&D Program of China (2022YFA1602200, 2022YFA1602400), and the National Natural Science Foundation of China (No. 12235003). We thank the staff from SIOM for providing the PW laser system in excellent conditions. We are grateful to Xiaobin Xia and Weidong Shen from the Department of Nuclear and Radiation Safety in the Shanghai Institute of Applied Physics (SINAP) for providing the TASLIMAGE Radon and Neutron dosimetry system. We acknowledge Zuixia He from SINAP for the SEM imaging on our targets. We also thank Wenjun Ma, Defeng Kong, and Xueqing Yan from Peking University for their early cooperation on D-D fusion in laser induced nanowire-array targets, which benefits this work a lot. We thank professor Wenqing Shen from the Shanghai Advanced Research Institute (SARI) for long term support in this experiment.

[1] H. W. Becker, C. Rolfs, and H. P. Trautvetter, Zeitschrift für Physik A Atomic Nuclei **327**, 341.
[2] R. E. Segel, S. S. Hanna, and R. G. Allas, Phys. Rev. **139**, B818 (1965).
[3] W. Nevins and R. Swain, Nuclear Fusion **40**, 865 (2000).
[4] S. Stave, M. Ahmed, R. France, S. Henshaw, B. Müller, B. Perdue, R. Prior, M. Spraker, and H. Weller, Physics Letters B **696**, 26 (2011).
[5] A. M. Boesgaard, C. P. Deliyannis, and A. Steinhauer, The Astrophysical Journal **621**, 991 (2004).
[6] J. Martinez-Val, S. Eliezer, M. Piera, and G. Velarde, Physics Letters A **216**, 142 (1996).
[7] D. Moreau, Nuclear Fusion **17**, 13 (1977).
[8] S. Eliezer and J. M. Martínez-Val, Laser and Particle Beams **16**, 581–598 (1998).
[9] H. Hora, G. Miley, M. Ghoranneviss, B. Malekynia, and N. Azizi, Optics Communications **282**, 4124 (2009).
[10] W. M. Nevins, Journal of Fusion Energy **17**, 25.
[11] H. Hora, S. Eliezer, G. Kirchhoff, N. Nissim, J. Wang, P. Lalousis, Y. Xu, G. Miley, J. Martinez-Val, W. McKenzie, and et al., Laser and Particle Beams **35**, 730–740 (2017).
[12] X. Ning, T. Liang, D. Wu, S. Liu, Y. Liu, T. Hu, Z. Sheng, J. Ren, B. Jiang, Y. Zhao, and et al., Laser and Particle Beams **2022**, e8 (2022).
[13] V. S. Belyaev, A. P. Matafonov, V. I. Vinogradov, V. P. Krainov, V. S. Lisitsa, A. Roussetski, G. N. Ignatyev, and V. P. Andrianov, Physical review. E **72 2 Pt 2**, 026406 (2005).
[14] C. Labaune, C. Baccou, S. Depierreux, C. Goyon, G. Loisel, V. Yahia, and J. Rafelski, Nature Communications **4**, 2506.
[15] A. Picciotto, D. Margarone, A. Velyhan, P. Bellutti, J. Krasa, A. Szydlowsky, G. Bertuccio, Y. Shi, A. Mangione, J. Prokupek, A. Malinowska, E. Krousky, J. Ullschmied, L. Laska, M. Kucharik, and G. Korn, Phys. Rev. X **4**, 031030 (2014).
[16] L. Giuffrida, F. Belloni, D. Margarone, G. Petringa, G. Milluzzo, V. Scuderi, A. Velyhan, M. Rosinski, A. Picciotto, M. Kucharik, J. Dostal, R. Dudzak, J. Krasa, V. Istokskaia, R. Catalano, S. Tudisco, C. Verona, K. Jungwirth, P. Bellutti, G. Korn, and G. A. P. Cirrone, Phys. Rev. E **101**, 013204 (2020).
[17] J. Bonvalet, P. Nicolaï, D. Raffestin, E. D'humieres, D. Batani, V. Tikhonchuk, V. Kantarelou, L. Giuffrida, M. Tosca, G. Korn, A. Picciotto, A. Morace, Y. Abe, Y. Arikawa, S. Fujioka, Y. Fukuda, Y. Kuramitsu, H. Habara, and D. Margarone, Phys. Rev. E **103**, 053202 (2021).
[18] D. Margarone, J. Bonvalet, L. Giuffrida, A. Morace, V. Kantarelou, M. Tosca, D. Raffestin, P. Nicolai, A. Picciotto, Y. Abe, Y. Arikawa, S. Fujioka, Y. Fukuda, Y. Kuramitsu, H. Habara, and D. Batani, Applied Sciences **12** (2022), 10.3390/app12031444.
[19] D. Kong, S. Xu, Y. Shou, Y. Gao, Z. Mei, Z. Pan, Z. Liu, Z. Cao, Y. Liang, Z. Peng, and et al., Laser and Particle Beams **2022**, e7 (2022).
[20] Y. Zhang, Z. Zhang, Y. Dong, K. Fang, H. Gu, Y. Dai, W. Qi, Z. Deng, X. Zhang, L. Yang, F. Lu, Z. Huang, K. Zhou, Y. Wu, W. Zhou, F. Liu, G. Zhang, B. Li, X. Zhao, X. Yuan, C. Wang, and Y. Li, "Enhanced α particle generation via proton-boron fusion reactions in laser-modulated plasma," (2024), arXiv:2401.07253 [physics.plasm-ph].

[21] M. A. Purvis, V. N. Shlyaptsev, R. Hollinger, C. Bargsten, A. Pukhov, A. Prieto, Y. Wang, B. M. Luther, L. Yin, S. Wang, and J. J. Rocca, Nature Photonics **7**, 796.

[22] L. Fedeli, A. Formenti, L. Cialfi, A. Pazzaglia, and M. Passoni, Scientific Reports **8**, 3834.

[23] J. Park, R. Tommasini, R. Shepherd, R. A. London, C. Bargsten, R. Hollinger, M. G. Capeluto, V. N. Shlyaptsev, M. P. Hill, V. Kaymak, C. Baumann, A. Pukhov, D. Cloyne, R. Costa, J. Hunter, S. Maricle, J. Moody, and J. J. Rocca, Physics of Plasmas **28**, 023302 (2021).

[24] E. Eftekhari-Zadeh, M. S. Blümcke, Z. Samsonova, R. Loetzsch, I. Uschmann, M. Zapf, C. Ronning, O. N. Rosmej, D. Kartashov, and C. Spielmann, Physics of Plasmas **29**, 013301 (2022).

[25] V. Kaymak, A. Pukhov, V. N. Shlyaptsev, and J. J. Rocca, Phys. Rev. Lett. **117**, 035004 (2016).

[26] W. H. Bennett, Physical Review **45**, 890 (1934).

[27] H. Hora and P. S. Ray, Zeitschrift für Naturforschung A **33**, 890 (1978).

[28] H. Hora, S. Eliezer, N. Nissim, and P. Lalousis, Matter and Radiation at Extremes **2**, 177 (2017).

[29] A. Curtis, C. Calvi, J. Tinsley, R. Hollinger, V. Kaymak, A. Pukhov, S. Wang, A. Rockwood, Y. Wang, V. N. Shlyaptsev, and J. J. Rocca, Nature Communications **9**, 1077.

[30] A. Curtis, R. Hollinger, C. Calvi, S. Wang, S. Huanyu, Y. Wang, A. Pukhov, V. Kaymak, C. Baumann, J. Tinsley, V. N. Shlyaptsev, and J. J. Rocca, Phys. Rev. Res. **3**, 043181 (2021).

[31] X. Liang, Y. Leng, C. Wang, C. Li, L. Lin, B. Zhao, Y. Jiang, X. Lu, M. Hu, C. Zhang, H. Lu, D. Yin, Y. Jiang, X. Lu, H. Wei, J. Zhu, R. Li, and Z. Xu, Opt. Express **15**, 15335 (2007).

[32] Y. Chu, X. Liang, L. Yu, Y. Xu, L. Xu, L. Ma, X. Lu, Y. Liu, Y. Leng, R. Li, and Z. Xu, Opt. Express **21**, 29231 (2013).

[33] X. Lu, H. Zhang, J. Li, and Y. Leng, Opt. Lett. **46**, 5320 (2021).

[34] Y.-F. He, X.-F. Xi, S.-L. Guo, B. Guo, C.-Y. He, F.-L. Liu, D. Wu, J.-H. Wei, W.-S. Yang, L.-H. Wang, D.-H. Zhang, M.-L. Qiu, G.-F. Wang, C.-Y. Li, and X.-F. Lan, Nuclear Science and Techniques **31**, 42 (2020).

[35] E. M. Awad, M. A. Rana, and M. A. Al-Jubbori, Nuclear Science and Techniques **31**, 118 (2020).

[36] P. Wang, X. Deng, Z. Ma, C. Fu, L. Fan, Q. Wang, J. Xu, T. Xu, L. Ji, B. Shen, Y. Liu, X. Cao, G. Zhang, and Y. Ma, Frontiers in Physics **11** (2023), 10.3389/fphy.2023.1166347.

[37] Y. Zhang, H.-W. Wang, Y.-G. Ma, L.-X. Liu, X.-G. Cao, G.-T. Fan, G.-Q. Zhang, and D.-Q. Fang, Nuclear Science and Techniques **30**, 87 (2019).

[38] J. F. Ziegler, Nuclear Instruments and Methods in Physics Research Section B: Beam Interactions with Materials and Atoms **219-220**, 1027 (2004), proceedings of the Sixteenth International Conference on Ion Beam Analysis.

[39] P. Hu, Z.-G. Ma, K. Zhao, G.-Q. Zhang, D.-Q. Fang, B.-R. Wei, C.-B. Fu, and Y.-G. Ma, Nuclear Science and Techniques **32**, 58 (2021).

[40] L. Fan, T. Xu, Q. Wang, J. Xu, G. Zhang, P. Wang, C. Fu, Z. Ma, X. Deng, Y. Ma, S. Li, X. Lu, J. Li, R. Xu, C. Wang, X. Liang, Y. Leng, B. Shen, L. Ji, and R. Li, Frontiers in Physics **11** (2023), 10.3389/fphy.2023.1167927.

[41] D. Kong, G. Zhang, Y. Shou, S. Xu, Z. Mei, Z. Cao, Z. Pan, P. Wang, G. Qi, Y. Lou, Z. Ma, H. Lan, W. Wang, Y. Li, P. Rubovic, M. Veselsky, A. Bonasera, J. Zhao, Y. Geng, Y. Zhao, C. Fu, W. Luo, Y. Ma, X. Yan, and W. Ma, Matter and Radiation at Extremes **7**, 064403 (2022).

[42] J. Derouillat, A. Beck, F. Perez, T. Vinci, M. Chiaramello, A. Grassi, M. Flé, G. Bouchard, I. Plotnikov, N. Aunai, J. Dargent, C. Riconda, and M. Grech, Comput. Phys. Commun. **222**, 351 (2018).

[43] D. P. Higginson, A. Link, and A. Schmidt, Journal of Computational Physics **388**, 439 (2019).

[44] D. P. Higginson, I. Holod, and A. Link, Journal of Computational Physics **413**, 109450 (2020).

[45] V. Kaymak, A. Pukhov, V. N. Shlyaptsev, and J. J. Rocca, Phys. Rev. Lett. **117**, 035004 (2016).

[46] J. J. Rocca, M. G. Capeluto, R. C. Hollinger, S. Wang, Y. Wang, G. R. Kumar, A. D. Lad, A. Pukhov, and V. N. Shlyaptsev, Optica **11**, 437 (2024).

[47] B. Wu, Z. Fan, D. Ye, T. Ye, C. Gao, C. Yu, X. Xu, C. Zhang, and J. Liu, Phys. Rev. C **109**, 064615 (2024).